INFLUENCE OF TEMPERATURE AND PLASTIC DEFORMATION ON AA2024 T3 FRICTION STIR WELDED JOINT MICROSTRUCTURE

by

Darko M. VELJIĆ[a*], Nenad A. RADOVIĆ[b], Marko P. RAKIN[b], Aleksandar S. SEDMAK[c], Bojan I. MEDJO[b], Mihailo R. MRDAK[a], and Darko R. BAJIĆ[d]

[a] Innovation Center, Faculty of Technology and Metallurgy, Belgrade, Serbia
[b] Faculty of Technology and Metallurgy, University of Belgrade, Belgrade, Serbia
[c] Faculty of Mechanical Engineering, University of Belgrade, Belgrade, Serbia
[d] Faculty of Mechanical Engineering, University of Montenegro, Montenegro

Original scientific paper
https://doi.org/10.2298/TSCI220621162V

This paper deals with analysis and comparison of the equivalent plastic strain and temperature fields in the aluminium alloy 2024 T3 (AA2024 T3) joint, with macro/microstructure appearance and hardness profile. In the alloys hardened by heat treatment, grain size and particle size of the precipitate are functions of equivalent plastic strain, strain rate and temperature. By analysing the equivalent plastic strain fields and temperature fields it is possible, to some extent, to capture the effect of welding parameters and thermo-mechanical conditions on grain structure, and therefore hardness and strength in the welded joint. A coupled thermo-mechanical model is applied to study the material behaviour during the linear welding stage of friction stir welding. The 3-D finite element model has been created in ABAQUS/EXPLICIT software using the Johnson-Cook material law. The values of thermo-mechanical quantities during the welding stage are obtained from the numerical model and shown as distributions across the joint. The obtained values of these quantities are related to the microstructure of the joint zones and hardness distribution, and this relation is discussed.

Key words: *AA2024 T3, friction stir welding, numerical simulation, equivalent plastic strain field, temperature field, hardness, microstructur*e

Introduction

The basis of the physical process of friction stir welding (FSW), fig. 1, is stirring of the material near the edges of two metal pieces in contact, at sufficiently high temperature. The working part of the welding tool consists of two parts: the cylinder and the pin (the pin is positioned under the cylinder). One of the tool movements is rotation, with prescribed rotation speed, but the tool is also exposed to additional vertical plunging force. This means that the contact with the working material is established, and the friction at this contact area leads to the heat generation. This heat must be sufficient to create conditions for thermo-mechanical solid state processing, without melting. This way, the conditions for joining (mixing) of the materials from the two metal pieces are established in the significantly heated zone. As a con-

* Corresponding author, e-mail: veljic.darko@gmail.com

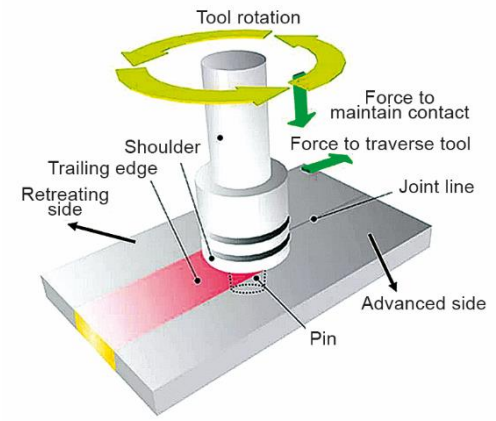

Figure 1. Schematic illustration of FSW process [9]

sequence of the action of the tool, *i.e.* both tool shoulder and pin, the joint of the two pieces is obtained. Also, significant plastic deformation occurs during the stirring process, therefore, this process consists of all elements which form the basis of high-temperature thermo-mechanical processing. During the deformation and recrystallization (static and/or dynamic), a very intensive decrease of grain size occurs in the welded joint microstructure, [1, 2]. Hence, the welded joint is often not a critical spot in the welded structure, because the microstructure which is formed does not contribute to the initiation of the cracks which are critical for welds: hot cracks, cold cracks, lamellar tearing or cracks caused by subsequent thermal treatment. Due to the lack of the liquid phase, no significant ductility reduction due to the presence of the rough dendrite structure in the weld metal or defects related to solidification are expected. Microstructure of the friction stir welded joints has been considered in numerous studies, *e.g.* [3, 4] for the similar joints (same base metals) and [5, 6] for dissimilar joints (different base metals). In addition to the microstructure of the joint zones, residual stresses also affect the integrity and load carrying capacity of the joint, as shown in [7, 8].

The conditions during the FSW are very complex, and include pronounced deformation (with an emphasis on plastic strains), high temperatures and flowing of the heated and softened material, as considered in many studies, including [10-19]. Knowledge about these conditions, which includes analytical and numerical calculations, can significantly decrease the amount of experimental work and enable optimization of the FSW process on a wide range of materials. Previous publications of the authors deal with different aspects of the linear welding stage of FSW, including the material properties effect [20] and velocity fields which occur in the material [21]. Also, the evolutions of force and temperature values during the welding are considered in [22]. Influence of welding parameters on the process itself or the joint properties is shown in [16, 23-25], while the effect of heat input, as another important topic for FSW, is considered in [26, 27].

Each welding process can result in some defects in the material and change of microstructure, with respect to this, FSW is advantageous in comparison with the melting processes. Also, one should take into account that welding is not always the last fabrication procedure during the production of some mechanical element. For example, cutting of the joint can cause additional surface defects, which is considered in [28] for water-jet cut joints. Also, the exploitation conditions affect the initiation and development of defects, which is analyzed on the example of wear in [29]. The authors report that the wear resistance of the joint zone is higher in comparison with the base metal. Pang *et al.* [30] studied the influence of deformation on another damage mechanism – corrosion of the FSW joint, through tensile testing procedure. Tensile testing was also the base for optimization of the FSW parameters in [31], where Taguchi method has been utilized on experimentally obtained results.

As mentioned previously, microstructure of the FSW joints has been previously considered in the literature, *e.g.* [1-6]. In most cases, experimental examinations are performed.

However, there are also studies where combined techniques are employed to predict the microstructure of the joint, such as [32] where cellular automaton model has been applied along with numerical model to predict the microstructure of the FSW joint, or [33] where spot friction stir weld has been considered. In this work, we present a correlation between the numerical results, expressed through the temperature and plastic strain fields, and the obtained microstructure and hardness across the joint. This enables a better insight into the thermomechanical state of the material, numerical results can be used to optimize the welding parameters and obtain the weld with appropriate microstructure. Analysis of the influence of the welding parameters to the joint strength, hardness and microstructure and comparison with the temperature, generated heat and plastic strains obtained from the numerical model contributes in predicting the weld properties with minimized experimental examinations. Also, the obtained temperature fields are an initial but important point for further analysis of the cooling process to the room temperature, which gives the residual stress fields in the welded joint.

Experimental work

The work pieces (plates prepared for welding) were produced from aluminium alloy EN AW 2024 T3, with thickness 3 mm and dimensions 180 × 65 mm, the fabrication of the joint was previously shown in [16, 34]. Basic material properties are given in tabs. 1 and 2. Alloy 2024 is one of the most often used high-strength aluminium alloys. Due to its high strength and excellent fatigue resistance, it is used for fabrication of mechanical parts which require a good strength-to-mass ratio. It is convenient for mechanical processing, but it is almost impossible to be welded by conventional welding processes with melting in the welding zone. It is commonly used in airspace engineering, transport industry and production of arms.

Table 1. Chemical composition of the base material [35]

Alloy	Content of element [w.t%]							
	Cu	Mg	Mn	Fe	Si	Zn	Ti	Al
2024 T3	4.80	1.41	0.72	0.28	0.13	0.07	0.15	bal.

Table 2. Material properties of Al 2024 T3 [35, 36]

Material properties	Value
Young's Modulus of Elasticity [GPa]	73.1
Poisson's Ratio [–]	0.33
Thermal Conductivity [$Wm^{-1}K^{-1}$]	121
Coefficient of thermal expansion [$°C^{-1}$]	24.7×10^{-6}
Density [kgm^{-3}]	2770
Specific heat capacity [$Jkg^{-1}°C^{-1}$]	875
Solidus [°C]	502
Liquidus [°C]	638

An adapted version of the CNC milling machine, Prvomajska AG400, 12 kW, is used for formation of the joints, [16, 34]. This was possible due to the similarity of the kine-

matics of the FSW and the milling process, with two main movements: rotation of the tool around the vertical axis and translation of the working table. Additionally, the vertical relative movement during the plunge stage is performed through the vertical upwards movement of the working table. The tool material is 56NiCrMoV7 tool steel, fig. 2. Left-hand thread on the tool pin stirs the plate material at the joining line, but it also pushes the material downward to the weld root, this forces the material to remain in the welding zone. Analysis of the influence of the tool pin geometry on the joint properties can be found in [37, 38].

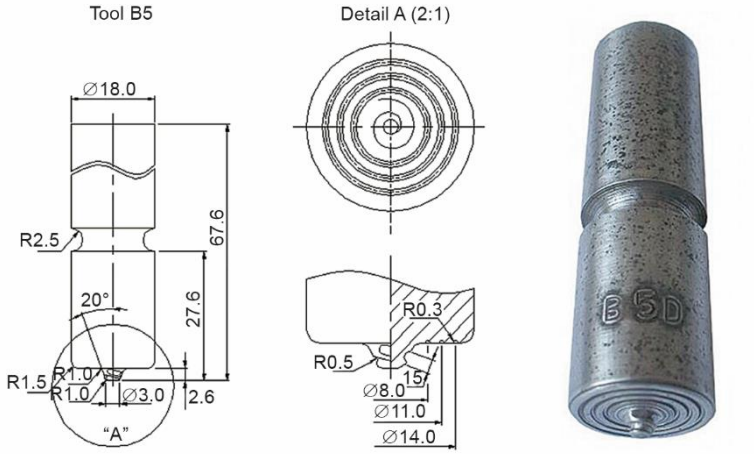

Figure 2. The FSW tool

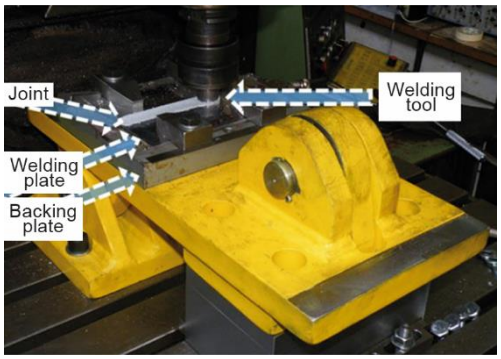

Figure 3. Welding equipment

Figure 3 shows the equipment and plates. Welding parameters are: tool rotation speed n_{rot} = 400 rpm, tool welding speed v = 40 mm per second.

After the plates had been successfully welded, the samples were cut in transversal direction (perpendicular to the joining line). These samples were subsequently used for examination of macrostructure, microstructure and hardness of the joint cross section (BM, HAZ – heat affected zone, TMAZ – thermo-mechanically affected zone, and the nugget), [16]. After polishing and etching, rinsing of the sample under water stream and submerging into alcohol, microstructure and macrostructure were examined. After that, the same sample was subjected to hardness measurement, by using the Vickers method (HV10), from retreating toward advancing side of the joint.

Numerical model

Numerical simulation is performed through finite element analysis, where joining of two plates with size 100 × 50 × 3 mm is considered, having in mind that the plate material is the same, they are represented as a single working plate with size 100 × 100 × 3 mm. The axis of symmetry coincides with the joining line. The model is shown in fig. 4, where the working

plate is given in longitudinal cross-section. The tool and the backing plate are modelled as rigid surfaces with three translation and three rotation freedom degrees, but without the thermal ones. The welding tool model has a cylindrical pin, which is an often used simplification in published studies dealing with FSW. The model (and different groups of the results, as mentioned in the Introduction section) are described in [13, 20-23], and some main notes are given here.

Through application of the Euler-Lagrange mesh adaptation technique, implemented in SIMULIA ABAQUS software package, it is possible to simulate the FSW process despite the extremely large plastic strains in the welding zone. The rotation speed and plunge speed of the welding tool are prescribed, and the translation of the tool along the welding line is simulated by defining the velocity of the Euler inflow surface. By defining the inflow and outflow Euler surfaces (side surfaces of the model, perpendicular to the welding line), the material is free to pass through the finite element mesh. The Euler inflow surface has prescribed ambient temperature of 25 °C.

The mesh, fig. 4, consists of 8-noded finite elements (C3D8RT). From this denotation of the element, it can be seen that mechanical and thermal quantities (displacement and temperature) have linear interpolation, and that reduced integration is applied. This is chosen in accordance with SIMULIA ABAQUS documentation [39], because formation of the Euler-Lagrange adaptive mesh requires first-order reduced-integration elements.

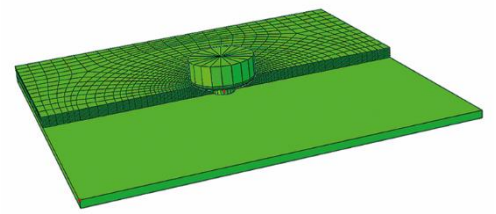

Figure 4. The model of the welding plate, tool and backing plate

A temperature and strain rate dependent material law (elastic-plastic Johnson-Cook law) is implemented, [40]. The parameters of this law for the analysed material are [41]: T_{melt} = 502 °C melting point or solidus temperature, T_{room} = 20 °C ambient temperature, A = 369 MPa, B = 684 MPa, n = 0.73, m = 1.7, and C = 0.0083 (the last five values are material/test constants for the Johnson-Cook model).

Since the backing plate is a rigid body and does not simulate the heat conduction, its influence is modelled by setting a high value of the heat transfer coefficient at the contact surface of the working plate and the backing one: 3000 W/m^2°C^1, in accordance with [13, 42]. As for the other (free) surfaces of the working plate, exposed to air at temperature 25 °C, the value is h = 10 W/m^2°C^1 [13, 42].

Results and discussion

In the aluminium alloys hardened by heat treatment, grain size and particle size of the precipitate are functions of equivalent plastic strain, strain rate and temperature. By analysing the equivalent plastic strain fields and temperature fields it is possible, to some extent, to study the influence of welding parameters on grain structure, and therefore on hardness and strength in the welded joint.

Figure 5 shows a parallel appearance of the macrostructure and microstructure of the cross section of the welded joint (weld zone and base metal), equivalent plastic strain field, temperature field and hardness profile. Based on all the experimental and numerical results given in this figure, an analysis of the weld zones is performed and presented in the following text.

After the numerical simulation of the FSW process, where the input parameters corresponded to the experiment (material and geometry of the welding plate, welding parameters, geometry of the tool and the backing plate, boundary conditions), the cross-section of the welded joint is shown alongside the calculated temperature and equivalent plastic strain fields, fig. 5. It should be noted that the microphotographs and the hardness are measured after the joint has been formed, while the temperature and strain fields are shown during the linear welding stage.

In the weld nugget zone, equivalent plastic strains are the highest, due to which the grain size is the smallest. In [43], it is shown that increase of the tool rotation speed leads to larger grains in the nugget of AA2024 T3 FSW joint. In relation to the retreating side, the value of plastic strain is greater on the advancing side, corresponding to the unsymmetrical appearance of the nugget. Unsymmetrical appearance means that the conditions on the advancing side differ from those on the retreating size. The difference can be seen by comparing the tool translation velocity and the rotational velocity of the tool circumference: they have the same direction on the advancing side and opposite direction on the retreating side, fig. 1. An almost imperceptible presence of precipitate in the nugget is an indication of completion of the thermo-mechanical regime.

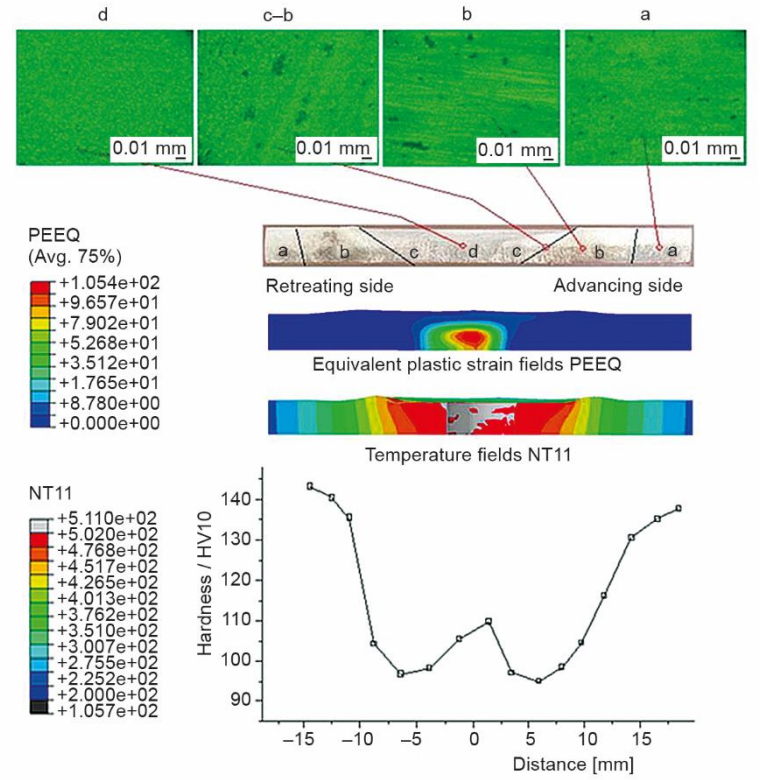

Figure 5. Comparison of macro/micro structure, hardness, temperature field and equivalent plastic strain field in the cross section of the welded joint; Alloy 2024 T3, welding speed v = 40 mm per minute, rotation speed n = 400 rpm; a – *base material, b – heat-affected zone (HAZ), c – thermo-mechanically affected zone (TMAZ), and d – weld nugget*
(*for color image see journal web site*)

In the TMAZ, smaller plastic strain is present, so the grains are larger relative to the nugget and precipitate is noticeably isolated due to high temperatures. The number of coarser precipitate particles increases at the expense of reducing the number of fine particles.

In the HAZ, the value of plastic strain is negligible. In the vicinity of the TMAZ, rough (coarse) precipitate is present due to the impact of high temperatures. The nature of distribution of precipitate in HAZ is in agreement with the findings in [24] obtained on friction stir welds produced from the same material. HAZ is a critical part of the welded joint with minimum hardness and tensile strength. With increasing distance from TMAZ, the impact of heat is less pronounced, *i.e.* the temperature drops and the number of larger particles decreases, which increases hardness.

Finally, we come to the base metal, where heat generated during the welding process has no influence on the structure. The structure of the base metal is characterized with a uniformly distributed fine precipitate and high hardness.

Due to the thermo-mechanical treatment of the nugget, *i.e.* the fine-grained structure, hardness of the nugget is greater than hardness of the HAZ, however, it is lower than hardness of the base metal.

Another view on the plastic strains will also be given here. In fig. 6, distribution of equivalent plastic strain along the joining line is shown. It can be seen that the maximum strains are obtained behind the tool pin, *i.e.* between the pin and the tool shoulder edge. Therefore, the strain distribution will be shown in the cross-section at this position, as marked in this figure.

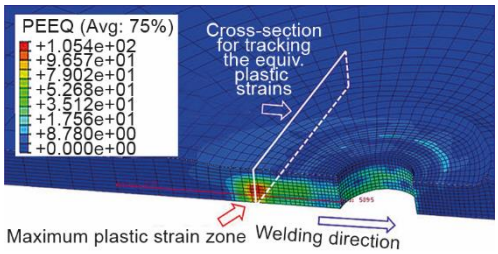

Figure 6. Equivalent plastic strain distribution – section along the joining line
(*for color image see journal web site)*)

The distribution of plastic strain in the cross-section is shown in fig. 7(a). It can be seen that the trend of this diagram is rather opposite to the hardness profile from fig. 5, *i.e.* the zones which were exposed to the highest strain values develop the lowest hardness. Distribution of temperature is given in fig. 7(b). It should be mentioned that the *distance* in fig. 7 is measured along the cross-section marked by white rectangle in fig. 6, which shows one half of the model.

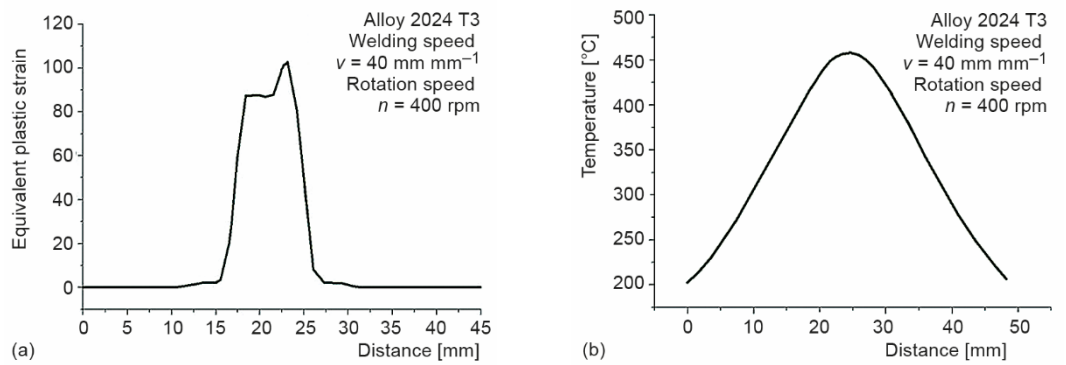

Figure 7. Equivalent plastic strain (a) and temperature and (b) distribution in the cross-section (marked in fig. 6)

Distribution of the stress values (equivalent von Mises stress) in the material is shown in figs. 8 and 9. Figure 8 corresponds to the end of the plunge stage, *i.e.* right before the linear welding stage is initiated. Therefore, high amount of heat input concentrated in the welding zone decreases the material strength and the stresses are very low.

During the welding, the stress values behind the tool increase, fig. 9, as the material cools down due to the tool translation movement along the joining line (from left to right in this figure). The position of the maximum stress is close to the position of the maximum plastic strain from fig. 6. It should be noted that the stresses are shown only during welding here, the residual stresses in the material after cooling will be considered elsewhere.

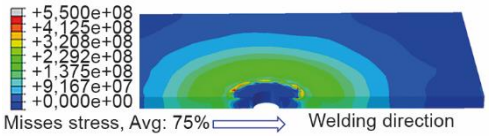

Figure 8. Equivalent von Mises stress field at the beginning of the linear welding stage – section along the joining line
(*for color image see journal web site*)

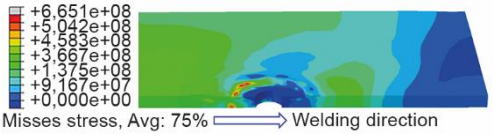

Figure 9. Equivalent von Mises stress field during the linear welding stage – section along the joining line
(*for color image see journal web site*)

With analysis of impact of welding parameters on strength and toughness of the joints, as well as on grain size and precipitate size in the welding zone, and comparing them with the equivalent plastic strain field, temperature field and the length of exposure to certain temperatures, conclusions which enable a proper quality assessment of the joints using numerical simulations can be drawn. Also, temperature fields which are shown in this work can be used in further simulation of the cooling process to room temperature, leading to residual stress fields. This is necessary for proper assessment of the load carrying capacity of the welded joint, and will be the topic of further research.

Conclusions

In this work, the relation between the microstructure and hardness of the friction stir welded joint and the fields of thermo-mechanical variables during the welding is considered. Thermo-mechanical variables (temperature and equivalent plastic strain, as well as equivalent von Mises stress) are obtained from the numerical model of the welding process. Regarding the weld nugget, a hardly noticeable presence of precipitates is an indication of the completed thermo-mechanical regime. In this zone, hardness is higher than in the HAZ, but lower than in the base metal; the equivalent plastic strain and temperature are the highest in the nugget. When the plastic strain is considered on both sides of the weld, higher values are obtained on the advancing side (when compared with the retreating side). The transition from TMAZ to HAZ results in rougher structure and coarse precipitates. This is the critical spot within the joint, characterized by minimal hardness values. The HAZ, where the influence of temperature decreases with approaching to the base metal, is therefore characterized by finer precipitate and increased hardness.

Acknowledgment

This work was supported by the Ministry of Education, Science and Technological Development of the Republic of Serbia (contr. 451-03-68/2022-14/200287, 451-03-68/2022-14/200135).

Nomenclature

- A – material parameter of the Johnson-Cook model [MPa]
- B – material parameter of the Johnson-Cook model [MPa]
- C – material parameter of the Johnson-Cook model [–]
- h – heat convection coefficient [$Wm^{-2}°C^{-1}$]
- m – material parameter of the Johnson-Cook model [–]
- n – material parameter of the Johnson-Cook model [–]
- n_{rot} – rotation speed of the tool [rpm]
- T_{melt} – solidus temperature [°C]
- T_{room} – ambient temperature [°C]
- v – welding speed [rpm]

References

[1] Orłowska, M., *et al.*, Local Changes in the Microstructure, Mechanical and Electrochemical Properties of Friction Stir Welded Joints from Aluminium of Varying Grain Size, *Journal of Materials Research and Technology, 15* (2021), Nov., pp. 5968-5987
[2] Ding, T., *et al.*, Effect of Welding Speed on Microstructure and Mechanical Properties of Al-Mg-Mn-Zr-Ti Alloy Sheet during Friction Stir Welding, *Transactions of Nonferrous Metals Society of China, 31* (2021), 12, pp. 3626-3642
[3] Chen, S., *et al.*, The Effect of Microstructure on the Mechanical Properties of Friction Stir Welded 5A06 Al Alloy, *Materials Science & Engineering A, 735* (2018), Sept., pp. 382-393
[4] Fall, A., *et al.*, Local Mechanical Properties, Microstructure, and Microtexture in Friction Stir Welded Ti-6Al-4V Alloy, *Materials Science & Engineering A, 749* (2019), Mar., pp. 166-175
[5] Yu, M., *et al.*, Microstructure and Mechanical Properties of Friction Stir Lap AA6061-Ti6Al4V Welds, *Journal of Materials Processing Technology, 270* (2019), Aug., pp. 274-284
[6] Mahto, R. P., *et al.*, Mechanism of Microstructure Evolution and Grain Growth in Friction Stir Welding of AA6061-T6 and AISI304 in Air and Water Media, *Materials Chemistry and Physics, 273* (2021), Nov., 125081
[7] Xu, W., *et al.*, Analysis of Residual Stresses in Thick Aluminum Friction Stir Welded Butt Joints, *Materials and Design, 32* (2011), 4, pp. 2000-2005
[8] Lombard, H., *et al.*, Effect of Process Parameters on the Residual Stresses in AA5083-H321 Friction Stir Welds, *Materials Science and Engineering A, 501* (2009), 1-2, pp. 119-124
[9] ***, Essai Group, https://www.essaii.com/friction-stir-welding-fsw-pros-cons/
[10] Song, M., Kovacevic, R., Numerical and Experimental Study of the Heat Transfer Process in Friction Stir Welding, *Journal of Engineering Manufacture, 217* (2003), 1, pp. 73-85
[11] Chen, C. M., Kovacevic, R., Finite Element Modelling of Friction Stir Welding – Thermal and Thermo-mechanical Analysis, *International Journal of Machine Tools & Manufacture, 43* (2003), 13, pp. 1319-1326
[12] Rodriguez, R. I., *et al.*, Microstructure and Mechanical Properties of Dissimilar Friction Stir Welding of 6061-To-7050 Aluminum Alloys, *Materials and Design, 83* (2015), Oct., pp. 60-65
[13] Veljic, D., *et al.*, A Coupled Thermo-Mechanical Model of Friction Stir Welding, *Thermal Science, 16* (2012), 2, pp. 527-534
[14] Veljić, D., *et al.*, Numerical Simulation of the Plunge Stage in Friction Stir Welding, *Structural Integrity and Life, 11* (2011), 2, pp. 131-134
[15] Janjic, M., *et al.*, Microstructural Evolution during Friction Stir Welding of AlSi1MgMn Alloy, *Metalurgija, 51* (2012), 1, pp. 29-33
[16] Eramah, A., *et al.*, Influence of Friction Stir Welding Parameters on Properties of 2024 T3 Aluminium Alloy Joints, *Thermal Science, 18* (2014), Suppl. 1, pp. S21-S28
[17] Mijajlovic, M., *et al.*, Experimental Studies of Parameters Affecting the Heat Generation in Friction Stir Welding Process, *Thermal Science, 16* (2012), Suppl. 2, pp. S351-S362
[18] Podržaj, P., *et al.*, Welding Defects at Friction Stir Welding, *Metalurgija, 54* (2015), 2, pp. 387-389
[19] Sarsilmaz, F., Relationship between Micro-Structure and Mechanical Properties of Dissimilar Aluminum Alloy Plates by Friction Stir Welding, *Thermal Science, 22* (2018), Suppl. 1, pp. S55-S66
[20] Veljic, D., *et al.*, Temperature Fields in Linear Stage of Friction Stir Welding – Effect of Different Material Properties, *Thermal Science, 23* (2019), 6B, pp. 3985-3992

[21] Veljic, D., *et al.*, Influence of Material Velocity on Heat Generation during Linear Welding Stage of Friction Stir Welding, *Thermal Science, 23* (2016), 5, pp. 1693-1701
[22] Veljic, D., *et al.*, Experimental and Numerical Thermo-Mechanical Analysis of Friction Stir Welding of High-Strength Aluminium Alloy, *Thermal Science, 17* (2013), Suppl. 1, pp. S28-S37
[23] Veljic, D., *et al.*, Thermo-Mechanical Analysis of Linear Welding Stage in Friction Stir Welding – Influence of Welding Parameters. *Thermal Science, 26* (2021), 3A, pp. 2125-2134
[24] Carlone, P., Palazzo, G., Influence of Process Parameters on Microstructure and Mechanical Properties in AA2024-T3 Friction Stir Welding, *Metallography, Microstructure, and Analysis, 2* (2013), 8, pp. 213-222
[25] Eramah, A., *et al.*, Impact Fracture Response of Friction Stir Welded Al-Mg Alloy, *Structural Integrity and Life, 13* (2013), 3, pp. 171-177
[26] Sedmak, A., *et al.*, Heat Input Effect of Friction Stir Welding on Aluminum Alloy AA 6061-T6 Welded Joint, *Thermal Science, 20* (2016), 2, pp. 637-641
[27] Ivanovic, I., *et al.*, Numerical Study of Transient Three-dimensional Heat Conduction Problem with a Moving Heat Source, *Thermal Science, 15* (2011), 1, pp. 257-266
[28] Kumar, R., *et al.*, Surface Integrity Analysis of Abrasive Water Jet-Cut Surfaces Of Friction Stir Welded Joints, *International Journal of Advanced Manufacturing Technology, 88* (2017), May, pp. 1687-1701
[29] Kumar, R., *et al.*, Wear Characteristics and Defects Analysis of Friction Stir Welded Joint of Aluminium Alloy 6061-T6, *Maintenance and Reliability, 18* (2016), 1, pp. 128-135
[30] Pang, Q., *et al.*, Effect of Deformation on the Corrosion Behavior of Friction Stir Welded Joints of 2024 Aluminum Alloy, *Materials, 15* (2022), 6, 2157
[31] Kumar, A., *et al.*, Optimization of FSW Parameters to Improve the Mechanical Properties of AA2024-T351 Similar Joints Using Taguchi Method, *Journal of Mechanical Engineering and Automation, 5* (2015), 3B, pp. 27-32
[32] Iqbal, M. P., *et al.*, Numerical Modelling of Microstructure in Friction Stir Welding of Aluminium Alloys *International Journal of Mechanical Sciences, 185* (2020), Nov., 105882
[33] Zhang, B., *et al.*, Thermo-Mechanical Simulation using Microstructure-Based Modeling of Friction Stir Spot Welded AA 6061-T6, *Journal of Manufacturing Processes, 37* (2019), Jan., pp. 71-81
[34] Veljic, D., *et al.*, Heat Generation during Plunge Stage in Friction Stir Welding, *Thermal Science, 17* (2013), 2, pp. 489-496
[35] ***, Certificate of Conformity, ALCOA International, Approved Certificate No. 47831, 1990
[36] ***, ASM International Aluminum 2024-T351 Data Sheet
[37] Radisavljevic, I., *et al.*, Influence of Pin Geometry on Mechanical and Structural Properties of Butt Friction Stir Welded 2024-T351 Aluminum Alloy, *Hemijska Industrija, 69* (2015), 3, pp. 323-330
[38] Hassanifard, S., *et al.*, The Effect of the Friction Stir Welding Tool Shape on Tensile Properties of Welded Al 6061-T6 Joints, *Materials Today Communications, 31* (2022), June, 103457
[39] ***, Dassault Systemes, Abaqus Analysis Manual, 2020
[40] Johnson, G. R., Cook, W. H., A Constitutive Model and Data for Metals Subjected to Large Strains, High Strain Rates and High Temperatures, *Proceedings*, 7th International Symposium on Ballistics, The Hague, The Netherlands, 1983, pp. 541-547
[41] Lesuer, D. R., Experimental Investigations of Material Models for Ti-6Al-4V Titanium and 2024-T3 Aluminium, Final Report, Department of Transportation, Washington DC, USA, 2000
[42] Schmidt, H., Hattel, J., A Local Model for the Thermomechanical Conditions in Friction Stir Welding, *Modelling & Simulation in Materials Science and Engineering, 13* (2005), 1, pp. 77-93
[43] Khodir, S. A., *et al.*, Microstructure and Mechanical Properties of Friction Stir Welded AA2024-T3 Aluminum Alloy, *Materials Transactions, 47* (2006), 1, pp. 185-193

Paper submitted: June 21, 2022
Paper revised: September 25, 2022
Paper accepted: October 4, 2022